Heliyon 6 (2020) e03784

Contents lists available at ScienceDirect

Heliyon

journal homepage: www.cell.com/heliyon

Research article

Synthesis of magnetite/silica nanocomposites from natural sand to create a drug delivery vehicle

Ahmad Taufiq [a,*], Ainun Nikmah [a], Arif Hidayat [a], Sunaryono Sunaryono [a], Nandang Mufti [a], Nurul Hidayat [a], Hendra Susanto [b]

[a] Department of Physics, Faculty of Mathematics and Natural Sciences, Universitas Negeri Malang, Jl. Semarang 5, Malang, 65145, Indonesia
[b] Department of Biology, Faculty of Mathematics and Natural Sciences, Universitas Negeri Malang, Jl. Semarang 5, Malang, 65145, Indonesia

ARTICLE INFO

Keywords:
Materials science
Nanotechnology
Biomedical engineering
Magnetite/silica
Nanocomposite
Natural sand
Doxorubicin
Drug delivery vehicle

ABSTRACT

In this study, we report the synthesis of the magnetite/silica nanocomposites and their structural and functional groups, magnetic properties, morphology, antimicrobial activity, and drug delivery performance. The X-ray diffraction characterization showed that magnetite formed a spinel phase and that silica formed an amorphous phase. The particle sizes of magnetite increased from 8.2 to 13.2 nm with increasing silica content, and the particles were observed to be superparamagnetic. The nanocomposites tended to agglomerate based on the scanning electron microscopy images. The antimicrobial activity of the magnetite/silica nanocomposites revealed that the increasing silica content increased the inhibition zones by 74%, 77%, and 143% in case of Gram-positive bacteria (*B. subtilis*), Gram-negative bacteria (*E. coli*), and fungus (*C. albicans*), respectively. Furthermore, doxorubicin was used as the model compound in the drug loading and release study, and drug loading was directly proportional to the silica content. Thus, the increasing silica content increased the drug loading owing to the increasing number of OH− bonds in silica, resulting in strong bonds with doxorubicin. Based on this study, the magnetite/silica nanocomposites could be applied as drug delivery vehicles.

1. Introduction

The incidence of cancer has been rapidly increasing in recent years and is currently considered to be a major global health threat [1]. More than 10 million cases of cancer are identified every year, and the predictions of the World Health Organization indicate that cancer will result in 13.1 million annual deaths by 2030 [2]. Further, various cancer treatment methods, such as radiation, chemotherapy, diagnostic treatment, and surgical intervention, have been developed to increase the survival rate. However, many of these methods, especially chemotherapy, affect other normally functioning organs owing to the applied therapeutic agents [3]. In addition, the chemotherapy drug agents harm the normal tissues because of their excessively high dosages [2]. Targeted drug delivery using nanoparticles as a platform would be very useful to prevent adverse effects from cancer treatment [4, 5].

Generally, materials used to develop drug delivery platforms include polymers, organic and magnetic materials, or a combination of them. These materials are subsequently combined with the cancer drug for targeted release in a cancerous environment [6, 7]. Currently, the most commonly used drug delivery platform is magnetite (Fe_3O_4) [8,9]. Magnetite is an oxide of iron and is the most commonly used material for medical applications because it is biocompatible as well as biodegradable and its surface modification is facile [10]. Magnetite nanoparticles have been extensively applied as magnetic scaffolds [11] for genetic material delivery [12], cell therapy [13], magnetic resonance imaging [14], and drug delivery [15]. Until now, magnetite has been synthesized using expensive precursors or raw materials. Therefore, in this study, the precursors used to synthesize magnetite have been obtained from abundant natural resources in the form of iron sand, which is significantly cheaper when compared with the commercial chemical precursors and reduces the production costs. However, the magnetite nanoparticles are unstable in air and agglomerate easily after their synthesis, significantly decreasing its magnetism and dispersibility. Therefore, the magnetite nanoparticles require further functionalization and modification with additional materials, including silica, polymers, carbon, luminescent materials, or other metal oxide absorbent materials [12].

Numerous methods have been developed to synthesize magnetite. For instance, Massart successfully synthesized magnetic nanoparticles to

* Corresponding author.
E-mail address: ahmad.taufiq.fmipa@um.ac.id (A. Taufiq).

https://doi.org/10.1016/j.heliyon.2020.e03784
Received 15 October 2019; Received in revised form 19 February 2020; Accepted 9 April 2020
2405-8440/© 2020 The Author(s). Published by Elsevier Ltd. This is an open access article under the CC BY-NC-ND license (http://creativecommons.org/licenses/by-nc-nd/4.0/).

produce magnetic fluids by the coprecipitation method in alkaline and acidic media using commercial ferric chloride and ferrous chloride as main precursors [16]. Kim *et al.* synthesized magnetite using the solvothermal method to scale up the close-packed superstructure of nanomaterials [17]. Further, other methods, including sol–gel–hydrothermal [18], wet chemical reduction [19], thermal decomposition [20], and Stöber [21, 22], have been successfully applied. However, the precursors used until now to synthesize magnetite were commercially available at high prices. Therefore, in this study, we formulated a more comfortable and cheaper synthesis method using natural materials in the form of iron sand.

In particular, silica was used for the functionalization of magnetite to develop a drug delivery system by maintaining nanoparticles in the solution state and increasing drug retention. Compared with pure magnetite, the incorporation of silica in a composite system results in improved bioaffinity and dispersion performance [23]. Moreover, the silica surface is chemically stable and biocompatible and can be easily functionalized for bioconjugation [24]. Silica coating of materials has been successfully applied in the fields of optics, erosion resistance, biosensing, biocatalysts, and biomedical devices [25, 26, 27, 28, 29]. Silica is not only a stabilizing factor but also provides sites for surface treatment with various ligands that are susceptible to the development of a drug delivery vehicle [26]. Among the advantages of the silica adding process, a relatively stable interface bond energy can be established using the nanoparticle core [30]. Silica can increase the nanoparticle solubility and stability of the drug delivery system toward the penetration of the cancer cell through the permeability effect and remain within the cancer cell because of its small size and small-volume pore and its large surface [31]. Further, the utilization of magnetite/silica in a composite system is advantageous because the size of the particles can be easily controlled, avoiding enhanced permeability and retention in the body [23]. In addition, under the external magnetic field, the drug loaded in the nanoparticles precisely reaches the target and improves the drug utilization performance [30]. Thus, the addition of silica to magnetite is considered to be the appropriate alternative to develop novel drug delivery systems. Doxorubicin hydrochloride (Dox) is a frequently used cancer drug. Dox is an anthracycline-based anticancer agent that can be used to treat various types of cancer [32]. However, Dox exhibits limited application owing to its toxicity in case of normal tissues, and the Dox degradation product is released into the fluid stream of the body, increasing the overall risk to the patient. Therefore, in terms of bioavailability, Dox has not fulfilled the clinical administration requirements [33]. Based on the perspective of environmental risk, it is necessary to control the release of Dox; furthermore, the efficient site-specific release of Dox on the target (cancer cell) is required to decrease the overall risk to normal body tissues.

Controlled Dox release has been successfully implemented previously using magnetite/silica. Previous studies have successfully considered the effects of various anticancer drugs, including Dox and paclitaxel (PTX), on magnetite/silica by controlling the pH of the solution. The efficiency and toxicity of the samples were also evaluated [34]. However, quantitatively, the resulting nanoparticle size was larger than 200 nm. Therefore, its use as an anticancer agent was limited because of the large size of the resulting particle [35]. Along with efficient drug loading and release, the particle size is a necessary requirement to obtain an ideal drug carrier. Hence, it is necessary to develop a simple nanoparticle synthesis method that can be used to generate small-sized products.

This study employed a simple coprecipitation method to synthesize magnetite and the sol–gel method to synthesize magnetite/silica nanocomposites. Compared with other methods, the sol–gel method can easily control the thickness of the silica shell, obtaining an excellent product shape [36]. In addition, this method is more time-efficient and can produce a more homogeneous and controlled surface when compared with the organosilane formation in magnetite [37]. Furthermore, a natural resource in the form of iron sand was employed as the leading source for the synthesis of the magnetite particles to reduce the synthesis cost. A schematic of the synthesis, drug loading, and drug release of the developed magnetite/silica nanocomposites is presented in Figure 1.

2. Materials and methods

Iron sand was obtained from Tulungagung Beach, Indonesia. Hydrochloric acid (HCl, 38%), ammonium hydroxide (NH_4OH, 25%), ethanol, doxorubicin, and tetraethyl orthosilicate (TEOS) were purchased from Sigma-Aldrich. The phosphate buffered saline (PBS) solution (Merck), distilled water, and deionized water were of analytical grade. Magnetite nanoparticles were synthesized via coprecipitation. In brief, the natural iron sand was washed using distilled water and was subsequently dried in the sun. The dry sand was then sifted to isolate the finest sand. Furthermore, the iron sand was extracted using a permanent magnet to separate impurities from the iron sand such as titanium, silica, calcium, and vanadium from iron sand to obtain the Fe_3O_4 powders with the purity of 99.5% [38]. In the next phase, iron sand (20 g) was diluted in HCl (58 ml) and stirred using a magnetic stirrer for 20 min to produce $FeCl_2$ and $FeCl_3$ solutions. The obtained solution (15 ml), which contained $FeCl_2$ and $FeCl_3$, reacted with ammonium hydroxide (20 ml) at room temperature. The mixture was stirred using a magnetic stirrer at 720 rpm for 35 min until a black magnetite nanoparticle precipitate was

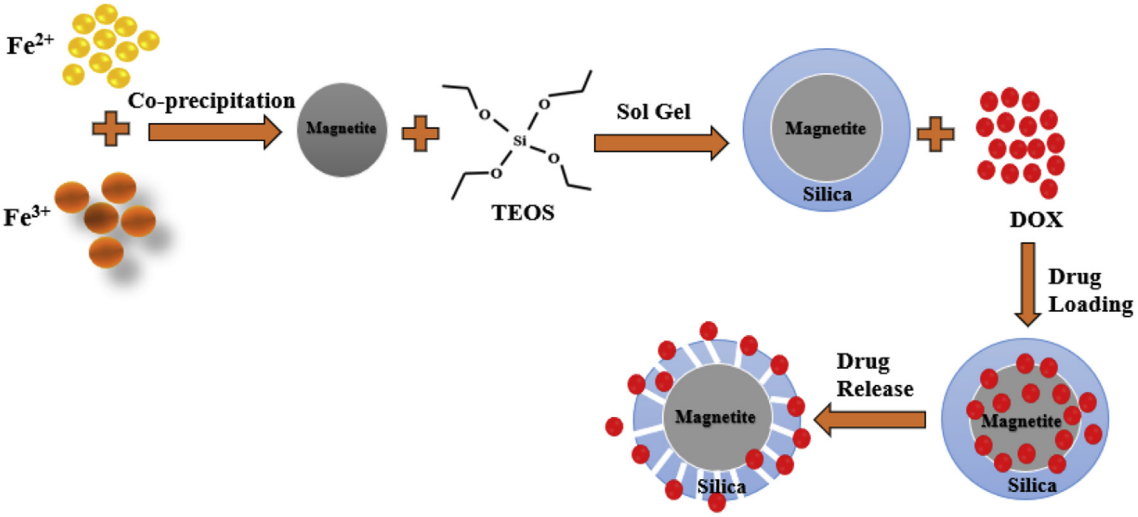

Figure 1. Schematic synthesis of the magnetite/silica nanocomposites.

formed. The black precipitate was washed using distilled water until a neutral pH was achieved. The black precipitates were collected using a filter paper to obtain magnetite nanoparticles, which were then dispersed into 50 ml of deionized water for further usage. The magnetite nanoparticles were subsequently modified using TEOS sequentially through the sol–gel method. The magnetite nanoparticle solution (20 ml) was added to ethanol (50 ml) and homogenized using the ultrasonication technique. The mixture reacted with ammonium hydroxide (4 ml) upon stirring for 30 min before the addition of TEOS (2 ml). In this study, the volume of TEOS varied for FS1 (2 ml of TEOS), FS2 (5 ml of TEOS), FS3 (8 ml of TEOS), and FS4 (11 ml of TEOS). The generated precipitate was washed using distilled water and ethanol several times. Subsequently, the obtained precipitate was filtered using a filter paper and heated to 80 °C for 2 h to obtain the magnetite/silica nanocomposite particles as the final product.

The obtained magnetite/silica nanocomposite particles were studied spectroscopically for their identification and property characterization. The formed crystal structure was investigated by X-ray diffraction (XRD) analysis, whereas the chemical composition was examined via X-ray fluorescence (XRF) spectroscopy. Fourier-transform infrared (FTIR) spectroscopy was conducted to explore the formed chemical bonds. Scanning electron microscopy (SEM) and energy dispersive X-ray analyzer (EDX) were employed to investigate the morphology and elemental composition of the samples. Furthermore, a vibrating sample magnetometer (VSM) was used to study the magnetic properties of the samples. To examine their potential applications with respect to the biomedical field, the response of the obtained nanoparticles to malignant pathogens was investigated. The antimicrobial (antibacterial and antifungal activities) characterization of the obtained nanocomposites was performed using a diffusion method. The apparent zone diameter was measured to identify the response of the nanoparticles toward microbial growth inhibition. The microbes used in this work included Gram-positive bacteria (*B. subtilis*), Gram-negative bacteria (*E. coli*), and *C. albicans*. Each sample was prepared by dissolving magnetite/silica (0.5 g) in DMSO (10 ml). The mixture was stirred using a magnetic stirrer for 10 min to obtain a homogenous solution. The mixed nanocomposites and DMSO (5 µl) were injected into suitable holes with a 5-mm diameter and 4-mm depth, which were inoculated with bacteria and incubated for 24 h. A similar process was also applied for the antifungal characterization of *C. albicans*. However, the medium used was Saboround Dextrose Agar.

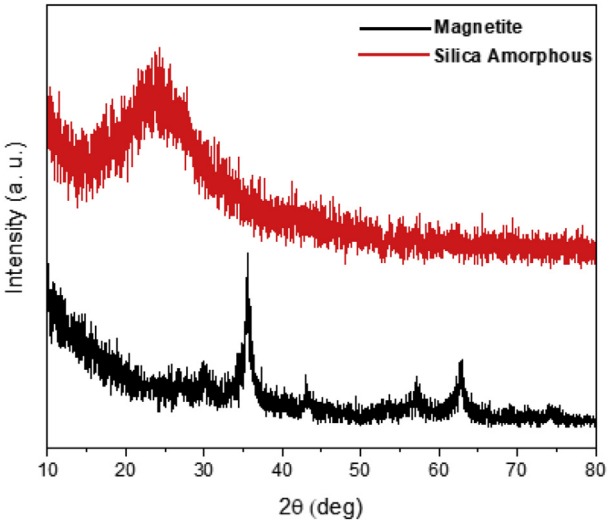

Figure 2. XRD patterns of the magnetite and amorphous silica.

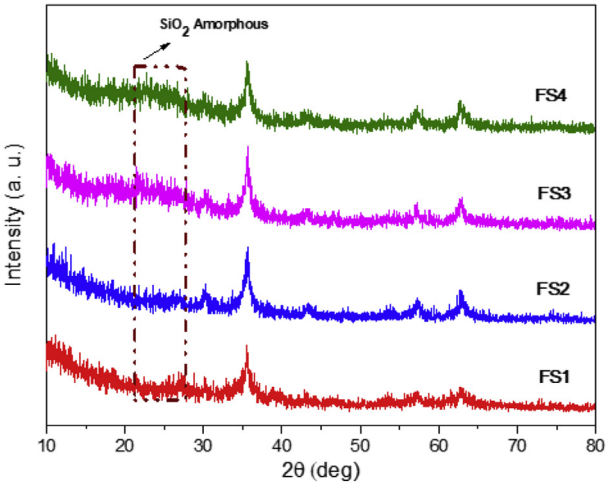

Figure 3. XRD patterns of the magnetite/silica nanocomposites.

Table 1. Elemental composition of the magnetite/silica nanocomposites by XRF.

Element	FS1 (wt%)	FS2 (wt%)	FS3 (wt%)	FS4 (wt%)
Si	7.4 ± 0.2	7.9 ± 0.5	28.3 ± 1.2	31.4 ± 1.8
Fe	92.6 ± 1.5	92.1 ± 1.5	71.7 ± 0.9	68.6 ± 0.7

Table 2. Particle size of Fe_3O_4 in the magnetite/silica nanocomposites.

Parameter	Magnetite	FS1	FS2	FS3	FS4
Particle size (nm)	8.2 ± 0.2	8.9 ± 0.2	9.9 ± 0.2	12.9 ± 0.3	13.2 ± 0.4

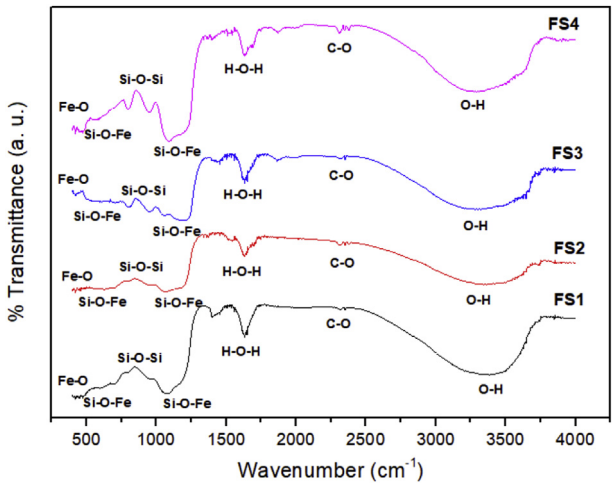

Figure 4. FTIR spectra of the magnetite/silica nanocomposites.

Table 3. Characteristic chemical bond vibrations of the magnetite/silica nanocomposites.

Sample	Functional group	Wavenumber (cm^{-1})	References
Magnetite	Fe–O stretching	459–500	[40, 45, 46]
	O–H stretching	3294–3464	[45, 46, 47, 48]
	C–O vibration	2360	[49, 50]
Silica	Antisymmetric Si–O–Si vibration	1078–1086	[42, 51, 52]
	Symmetric stretching Si–O–Si vibration	950	[42, 51, 52]
Magnetite/silica nanocomposites	Fe–O–Si vibration	541–575	[42, 48]
	H–O–H	1645	[42]

In the drug loading experiment, magnetite/silica nanocomposites (20 mg) were added to a 10-ml solution containing 3 mL of Dox (0.5 g/mL) and 7 mL of PBS solution, followed by stirring for 8 h at a speed of 700 rpm in the dark. The Dox-loaded nanoparticles (Magnetite–Dox) (NPs + Dox + PBS) were centrifuged at 6000 rpm for 20 min, and the generated supernatant was eliminated to observe the unloaded Dox via UV-Vis spectroscopy. The initial reaction solution was characterized by UV-Vis and analyzed at 480 nm. The centrifugation pellet contained

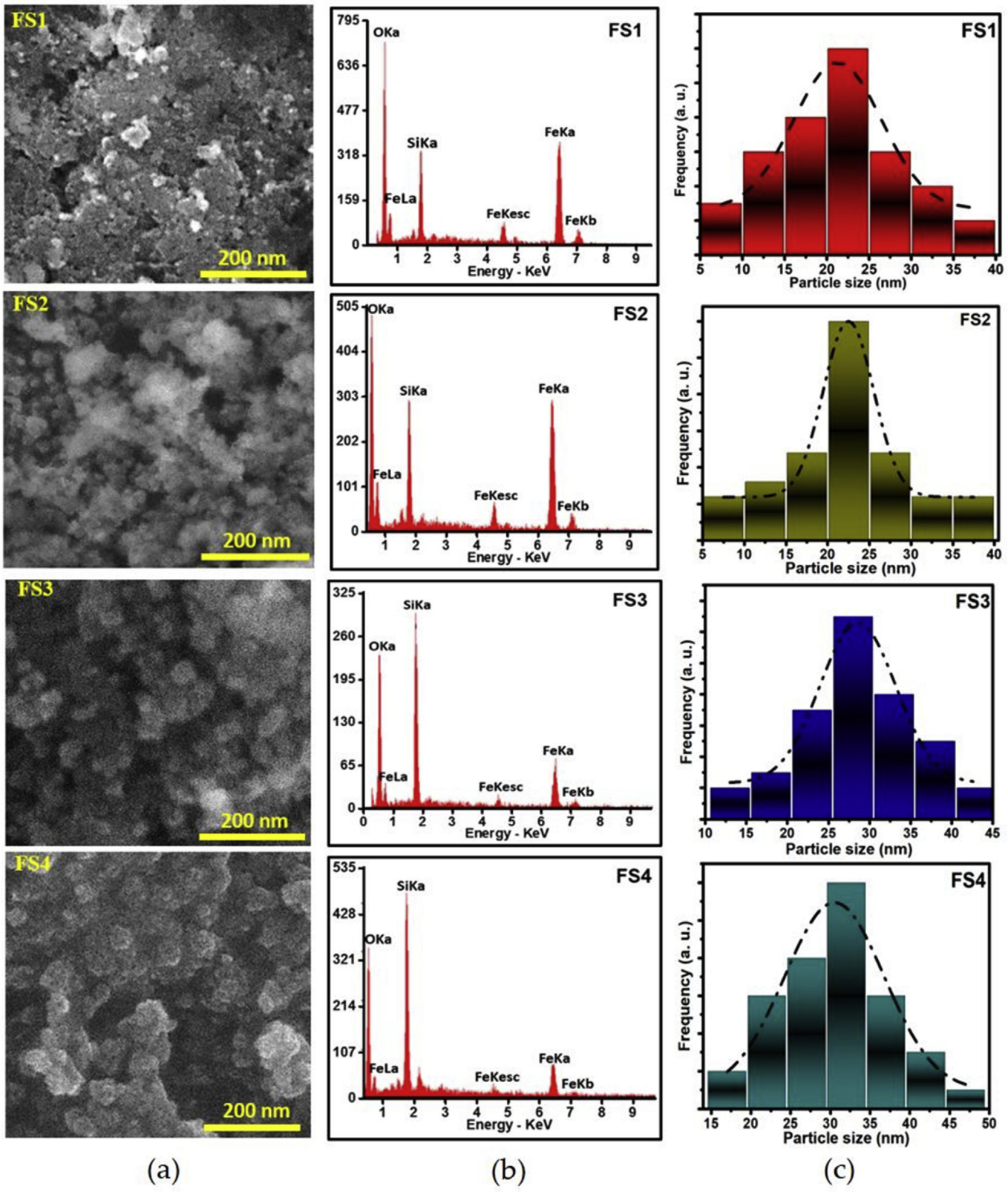

Figure 5. (a) SEM images, (b) EDX spectra, and (c) particle size distributions of the samples FS1, FS2, FS3, and FS4. The SiKa, OKa, FeKa, FeLa, FeKb, and FeKesc represent the elemental contents (Si, O, and Fe) of the magnetite/silica nanocomposites.

Dox-loaded nanoparticles and was used for release characterization. For the in vitro release of the Dox experiment, a PBS solution was prepared to simulate the body-tissue liquid. In particular, magnetite–Dox (5 mg) was dispersed into PBS (7 ml) and stirred at 720 rpm at different time intervals. A 3-ml solution inside the release medium was characterized using UV-Vis and subsequently analyzed at a wavelength of 480 nm. Furthermore, a 3-ml fresh PBS solution was added to the solution to serve as a substitute for the 3-ml solution and maintain the total volume.

3. Results and discussion

The phase and purity of the samples were characterized using XRD analysis. Figure 2 depicts the pure phase of magnetite and amorphous silica before combining them. All the magnetite diffraction peaks (30.36°, 35.44°, 43.27°, 57.59°, and 62.95°) could be observed at hkl fields of (220) (311) (400) (511), and (440), respectively. The single phase of magnetite has a spinel cubic structure with a fd-3m space group based on AMCSD No. 7766. The XRD peak of silica was observed at $2\theta =$ 22°–28° and identified to be amorphous silica. In this study, no significant changes were observed in case of the magnetite peaks after silica was added as shown in Figure 3. However, a new peak was identified at $2\theta = 22°–27°$, indicative of the presence of amorphous silica. Similar changes were observed in the previously obtained XRD patterns [39, 40].

Based on the elemental composition analysis (Table 1), the magnetite nanoparticles were combined with 7.4–31.4 wt% of Si. The silica diffraction peak was not visible in case of samples with low Si content (7.4–7.9 wt%). The slow addition of TEOS encouraged the growth of an extremely thin silica layer on the magnetite surface. With the addition of more TEOS, more silica was formed on the magnetite particles, which was observed as an increasing diffraction peak corresponding to amorphous silica [41, 42].

Furthermore, the particle size of magnetite before and after the addition of silica, which constituted the magnetite/silica nanocomposites, was calculated. The silica particle size could not be measured because the natural silica nanoparticles were amorphous. However, a quantitative estimation of the nanocomposite particle size was determined using the scanning electron microscopy (SEM) results based on the particle size distribution. The particle size (D) of magnetite can be calculated using the Debye–Scherrer equation (Eq. 1):

$$D = 0.9\lambda/\beta \cos\theta \tag{1}$$

where λ is the wavelength of the X-ray radiation, θ is the diffraction angle, and β is the full width at half maximum of the peak. The calculation results denoted a particle size of approximately 8.2–13.2 nm, as shown in Table 2. Furthermore, other researchers, such as Karimi *et al.*, synthesized magnetite/silica nanocomposites using commercial precursors and obtained particle sizes of approximately 80–108.5 nm [43]. Stjerndahl *et al.* obtained similar nanocomposites using a microemulsion method and obtained a particle size of approximately 56 nm [44].

Figure 4 depicts the FTIR spectra of the magnetite/silica nanocomposites with various silica concentrations. The characteristic vibrations for the chemical bonds in magnetite, silica, and the magnetite/silica nanocomposites are presented in Table 3. The following characteristic FTIR peaks of magnetite were observed. The Fe–O stretching vibration was observed at 459–500 cm^{-1}, the O–H vibration was observed on the magnetite surface at 3294–3464 cm^{-1}, and the C–O vibration was observed at 2360 cm^{-1}. The vibrations of Si (–O–Si, Si–O, and Si–O–Fe) confirmed the existence of silica in the samples. The antisymmetric vibration of Si–O–Si was observed at 1086 cm^{-1}, whereas the symmetric stretching vibration of Si–O–Si was observed at 950 cm^{-1}. The characteristic peak of the magnetite/silica bond, i.e., Fe–O–Si, was detected at 541–575 cm^{-1}. Interestingly, the penetration of the silanol group into samples indicated the successful formation of the silica/magnetite nanocomposites. In this study, water was detected in the samples with an H–O–H stretching peak at approximately 1645 cm^{-1} [42].

The SEM images, EDX spectra, and particle size distributions of the magnetite/silica nanocomposites are presented in Figure 5. EDX characterization of the samples confirmed the existence of the Fe (FeKa, FeKb, FeLa, and FeKesc), Si (SiKa), and O (OKa) atoms. The weight percentage of the Si contents in FS1 and FS2 was 12.8 and 13.4 wt%, respectively, whereas in FS3 and FS4 was 29.3 and 32.1 wt%, respectively. The EDX spectra of the samples at energies of 7 and 4.5 keV presented the peak intensities of FeKb [53, 54], FeKesc/TiKa [55], respectively. The presence of Ti in the samples originating from small impurities from iron sand as the main precursor [56]. Based on Figure 5, it was also known that the increasing TEOS composition tended to increase the particle size of the magnetite/silica nanocomposites. The increasing TEOS composition as the main source of silica increased the silica composition in the magnetite/silica nanocomposites. The quantitative analysis for the SEM images using lognormal distribution model revealed that the average particle sizes of the samples were of 21.3 ± 0.8, 22.5 ± 0.3, 28.3 ± 0.6, and 30.0 ± 0.8 nm for the respective FS1, FS2, FS3, FS4 samples. Visually, all samples tended to agglomerate originating from the surface interaction and magnetic forces of the nanoparticles [32].

The hysteresis curves were obtained using VSM to determine the magnetic properties of the samples are shown in Figure 6. Interestingly, in the magnetite, FS1, FS2, FS3, and FS4 samples, the remnant magnetization and coercivity field were approximately zero and demonstrated typical superparamagnetic properties [33, 46]. The hysteresis curves, which were fitted using the Langevin equation (Eq. 2) [46], is presented in Figure 7.

$$M = M_S L\left(\frac{\mu_P H}{K_B T}\right) + \chi H, \tag{2}$$

where M is the magnetization, T is the temperature, H is the applied magnetic field, k_B is the Boltzmann constant, μ_p is the average moment, and χ is the susceptibility. The saturation magnetization (Ms), remnant magnetization (Mr), χ values of the samples are presented in Table 4. Accordingly, pure magnetite exhibited the highest saturation magnetization value of approximately 30.3 emu/g. However, the saturation value decreased after silica was combined with the magnetite sample. The FS1 sample that contained the lowest silica amount had a saturation value of 21.6 emu/g. With increasing silica content in the sample, the saturation magnetization showed a significant decrease with values of 21.6, 11.5, 10.6, and 9.2 emu/g for FS1, FS2, FS3, and FS4, respectively. This

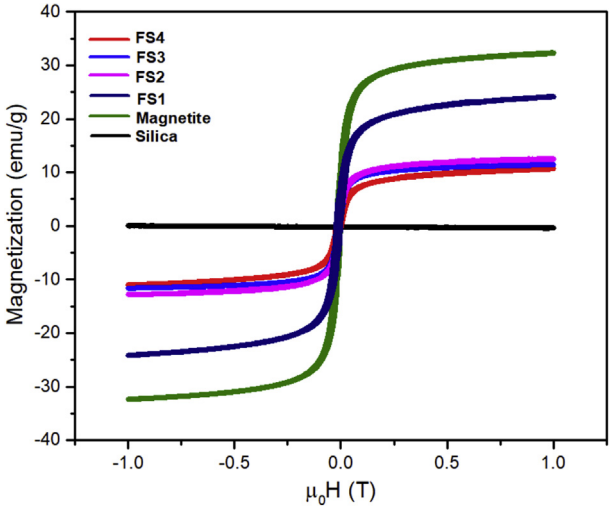

Figure 6. Hysteresis curves of the magnetite, silica, and magnetite/silica nanocomposites.

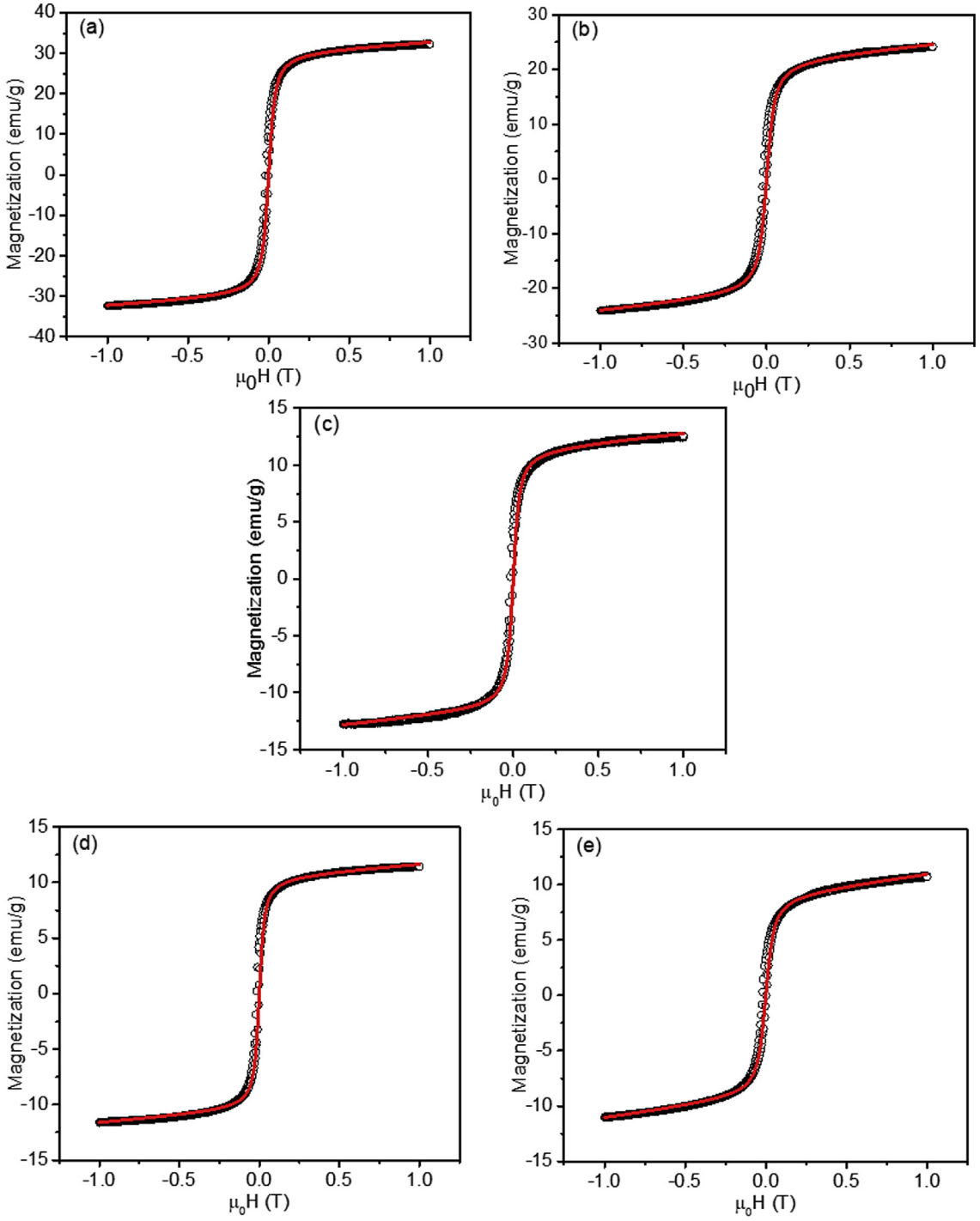

Figure 7. Fitted hysteresis curves of the samples (a) magnetite, (b) FS1, (c) FS2, (c) FS2, (d) FS3, (d) FS3, and (e) FS4. The *circles* represent the magnetization data, and the *solid lines* represent the fitting model using the Langevin equation.

Table 4. *Ms*, *Mr*, and χ values of the samples through magnetization data analysis.

Sample	*Ms* (emu/g)	*Mr* (emu/g)	χ	Magnetic moment (J/T)
Magnetite	30.3	0.23	3.1	6.7×10^{-18}
FS1	21.6	0.24	2.6	9.2×10^{-19}
FS2	11.5	0.02	1.5	8.9×10^{-19}
FS3	10.6	0.02	1.2	8.5×10^{-19}
FS4	9.2	0.06	2.0	8.1×10^{-19}

declining magnetization value was associated with the fact that silica is a non-magnetic material. The presence of silica on the magnetite surface reduced the interaction of the applied magnetic field with the intrinsic moments on the magnetite surface [46]. Therefore, the magnetic saturation value decreased with increasing silica content in the sample. Gao *et al.* proved that the saturation magnetization values ranged from 12 to 2.4 emu/g based on the magnetite/silica synthesis of TEOS variations using the Stöber method and that the saturation magnetization values decreased with the increasing composition of TEOS [24]. Other researchers, such as Duan *et al.*, reported a decrease in the saturation

magnetization value of the magnetite particles modified using O-phosphorylethanolamine [57].

Another magnitude of the magnetic properties that can be measured is the susceptibility value of the materials. Generally, the susceptibility of a material indicates its response or sensitivity to the applied external magnetic field. The measured susceptibility values (Table 4) tended to follow the same trend as that of the saturation magnetization. The higher the concentration of the added silica, the susceptibility value tended to be lower. According to theory, the increase in susceptibility is proportional to the increase in saturation magnetization, which can be mathematically explained using Eq. (2). The susceptibility value is directly proportional to the magnetization value. However, the decrease in the value of magnetization and susceptibility in a sample does not affect the paramagnetic properties of the material. All the composited exhibited perfect superparamagnetic properties. Therefore, the magnetite/silica nanocomposites are expected to be applied in several medical applications, especially as drug delivery vehicles.

The investigation of the bio–nano surface interactions are essential to ensure that the nanoparticles are safe for biomedical system applications. The examination of their tendency to inhibit bacteria is a preliminary characterization. Herein, the disinfection ability of the magnetite/silica nanocomposites before the loading process of Dox was investigated using Gram-positive bacteria (*B. subtilis*), Gram-negative bacteria (*E. coli*), and *C. albicans*.

The baseline inhibition values with respect to the microbes were established in the magnetite sample, with a silica composition of 0%. The polymer electronegative chemical groups in the bacterial membrane and the metal cation in magnetite are attracted to each other. The presence of such electrostatic forces on the entire bacterial cell surface can damage the cell wall [58]. In the FS1 to FS4 samples, the inhibition zones increased owing to the addition of silica. In this study, the silica nanoparticles serve as molecule connectors between magnetite and various microorganisms. The hybrid silica nanoparticles that coat magnetite have been proved to be considerably effective to kill bacteria [59]. The functionalization of silica nanoparticles with respect to magnetite is normally favorable to suppress magnetite agglomeration due to the magnetic dipole–dipole attraction [60]. The reduction of agglomeration increases the available surface area on the nanoparticles and the effectiveness of the antimicrobial activity.

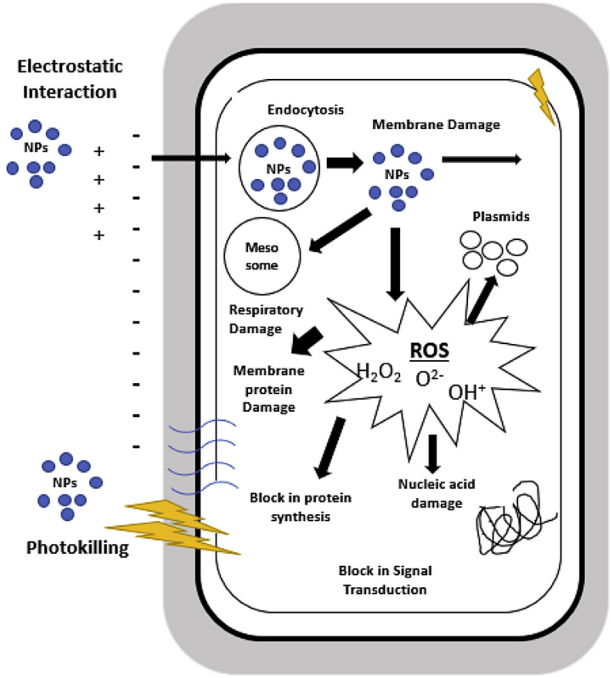

Figure 8. Mechanisms of cell damage by nanoparticles.

Theoretically, nanoparticles can increase the inhibition zone by easily penetrating the cell membranes and damage the intracellular functions to initiate cell death. Furthermore, the bonding between silica and cellular membrane can change the structure and permeability of the membrane. Thus, this nanoparticle-induced damage to the microbial cellular structure can cause leakage of the cellular content [58]. Once inside the cell, the primary mode of antimicrobial action by the nanoparticles is the production of reactive oxygen species (ROS) [61]. The mechanisms of cell damage that can be attributed to nanoparticles (NPs) are shown in Figure 8. Furthermore, based on Figure 9, the inhibition zone of the samples increased with increasing silica content. In the Gram-positive bacteria (*B. subtilis*), the inhibition zone increased by 74%, whereas in the Gram-negative bacteria (*E. coli*) and the antifungal bacteria (*C. albicans*), the inhibition zone was 77% and 143%, respectively. Therefore, the functionalization of nanoparticles with silica resulted in an excellent inhibition performance with respect to the three studied microbe species.

Dox loading on nanoparticle carriers was analyzed using UV-Vis over wavelengths of 200–900 nm. Figure 10 presents the UV-Vis spectra of the Dox-loaded magnetite/silica nanocomposites. The wavelength of SBF used in the loading process was observed to be 200–250 nm [62]. The Dox peaks were found at the wavelengths of 290 and 480 nm. In line with the results of this work, Cai and co-workers reported that the Dox peaks appeared at the wavelengths of 291 and 480 nm [32]. The Dox loading

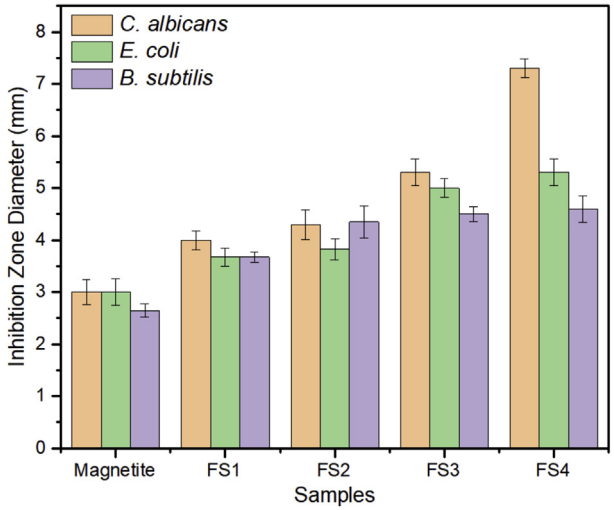

Figure 9. Inhibition zone diameter of the magnetite/silica nanocomposites.

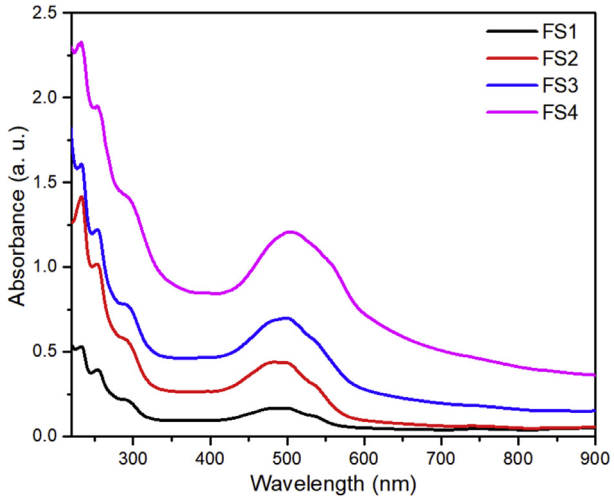

Figure 10. Dox loading profiles of the magnetite/silica nanocomposites.

profiles were also totally matched with the patterns testified by Li et al. [63]. Furthermore, the Dox loading profiles were different from the profiles of Fe_3O_4/SiO_2 composites without Dox, as reported by Gan et al. [64]. Therefore, the Dox loading profiles in this work revealed that the Dox was successfully loaded in the magnetite/silica nanocomposites. We reported these preliminary results, but the critical question of Dox loading will be fully treated in the near future.

Additionally, the Dox peak increased with respect to absorbance with an increase in the silica content of the carriers. Therefore, the higher the silica content, the higher will be the Dox absorbance peak [33]. In this case, the silanol group from silica acts to provide a binding site to other compounds [32], whereas the OH− silanol groups on the silica surface favor the Dox loading. Hence, the positive NH3+ group of the hydrophilic Dox develops a strong bond with OH− on the silica shell. Moreover, the number of OH− bonds of the silica excess that does not bind with water will result in a strong bond with Dox. Therefore, the absorbance of Dox increases as a function of the increased Dox loading [51, 65].

The efficiency of drug loading (L_e) with respect to the carrier can be calculated as follows:

$$\%L_e = \frac{m_0 - m_1}{m_0} \times 100\%, \quad (3)$$

where m_0 is the total Dox added to the reaction and m_1 is the amount of non-loaded Dox. Based on Eq. (3), the drug loading efficiency values of FS1, FS2, FS3, and FS4 were 58%, 63%, 65%, and 67%, respectively. Similar values were also reported by Mortazavi *et al.* [66].

The Dox release was also studied because the characteristics of drug release are extremely important to successfully develop a drug delivery system. Figure 11 depicts the cumulative release of Dox with time. A rapid drug release was observed for the FS1 sample in 25–100 min FS2 experienced a rapid release in 50–150 min, whereas for the FS3 and FS4 samples, the release occurred in 50–75 min and 25–75 min, respectively. Furthermore, Deepika *et al.* reported that an optimum release speed of 43.9% was achieved after the 15th min, with a silica layer thickness of 15 nm [67]. A high initial dose followed by a stable drug dose is generally beneficial for the administration of therapeutic drugs in the long run. Other researchers, such as Jiang *et al.*, investigated the change in the release rate of Fe_3O_4/SiO_2–Dox with pH variations and obtained an optimum release rate of 62.23% in 72 h [23]. In this study, the kinetic release showed long-term stable drug dosage. The Dox release profile showed different release rates during the first period, which was affected by the differing silica content. The Dox release speed was dependent on the silica content. In nanocomposites with high silica amounts, the Dox release speed was fast, similar to the increase in the observed loading rate with increasing silica content. The nanocomposites containing more silica should be more effective against cancer cells because more Dox can be delivered, damaging and killing the tumor cells more quickly [23]. Additionally, the silanol groups on the silica surface should serve as a coupling silane, facilitating drug loading and release [33].

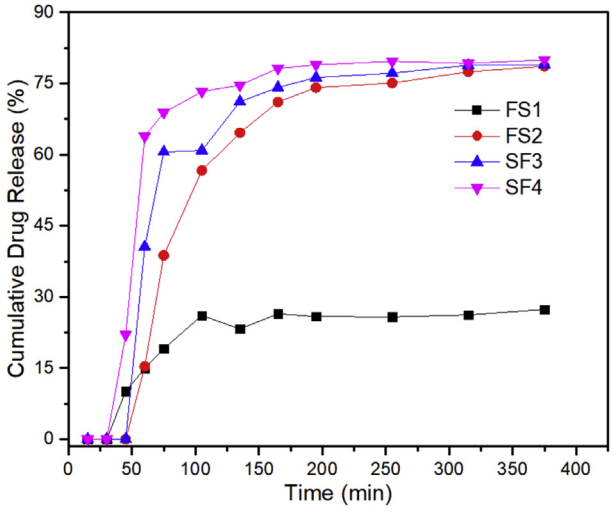

Figure 11. Cumulative drug release profiles of the magnetite/silica nanocomposites.

4. Conclusions

Magnetite/silica nanocomposites were successfully synthesized using the sol–gel method. The formation of magnetite/silica was confirmed using the XRD, XRF, and FTIR measurements. Based on SEM images, the particle size of the magnetite/silica nanocomposites was observed to be 21.3–30.0 nm. The obtained nanocomposites demonstrated superparamagnetic properties. The antimicrobial activity of the magnetite/silica nanocomposites with respect to *B. subtilis*, *E. coli*, and *C. albicans* was studied without Dox loading, and the increasing silica content increased the microbial inhibition zones by 74%, 77%, and 143%, respectively. In terms of drug loading and release, a positive correlation was observed between silica content and Dox loading. Fast Dox release could be observed within the initially 25–100 min; simultaneously, the release rate drastically decreased. Interestingly, the kinetic release study revealed that the drug dosage tended to remain stable for a sufficiently long period.

Declarations

Author contribution statement

Ahmad Taufiq: Conceived and designed the experiments; Analyzed and interpreted the data; Wrote the paper.

Ainun Nikmah: Performed the experiments; Wrote the paper.

Arif Hidayat: Contributed reagents, materials, analysis tools or data; Wrote the paper.

Sunaryono Sunaryono: Conceived and designed the experiments; Performed the experiments.

Nandang Mufti, Nurul Hidayat: Contributed reagents, materials, analysis tools or data.

Hendra Susanto: Performed the experiments.

Funding statement

This work was supported by DRPM KEMENRISETKDIKTI Republic of Indonesia (Grant No. 074/SP2H/LT/DRPM/2019).

Competing interest statement

The authors declare no conflict of interest.

Additional information

No additional information is available for this paper.

Acknowledgements

We would like to extend our sincere appreciation to the Central Laboratory of Universitas Negeri Malang for providing synthesis and characterization facilities.

References

[1] L.A. Torre, B. Trabert, C.E. DeSantis, K.D. Miller, G. Samimi, C.D. Runowicz, M.M. Gaudet, A. Jemal, R.L. Siegel, Ovarian cancer statistics, 2018, CA A Cancer J. Clin. 68 (2018) 284–296.

[2] S. Senapati, A.K. Mahanta, S. Kumar, P. Maiti, Controlled drug delivery vehicles for cancer treatment and their performance, Signal Transduct. Targeted Ther. 3 (2018) 7–26.

[3] W. Pon-On, T. Tithito, W. Maneeprakorn, T. Phenrat, I.-M. Tang, Investigation of magnetic silica with thermoresponsive chitosan coating for drug controlled release and magnetic hyperthermia application, Mater. Sci. Eng. C 97 (2019) 23–30.

[4] J.H. Adair, M.P. Parette, E.İ. Altınoğlu, M. Kester, Nanoparticulate alternatives for drug delivery, ACS Nano 4 (2010) 4967–4970.

[5] K. Park, Facing the truth about nanotechnology in drug delivery, ACS Nano 7 (2013) 7442–7447.

[6] S. Mura, J. Nicolas, P. Couvreur, Stimuli-responsive nanocarriers for drug delivery, Nat. Mater. 12 (2013) 991–1003.

[7] J. Yu, X. Chu, Y. Hou, Stimuli-responsive cancer therapy based on nanoparticles, Chem. Commun. 50 (2014) 11614–11630.

[8] M.-C. Liu, B. Liu, X.-Y. Sun, H.-C. Lin, J.-Z. Lu, S.-F. Jin, S.-Q. Yan, Y.-Y. Li, P. Zhao, Core/shell structured Fe3O4@TiO2-DNM nanospheres as multifunctional anticancer platform: chemotherapy and photodynamic therapy research, J. Nanosci. Nanotechnol. 18 (2018) 4445–4456.

[9] C. Xu, S. Sun, New forms of superparamagnetic nanoparticles for biomedical applications, Adv. Drug Deliv. Rev. 65 (2013) 732–743.

[10] N. Bukit, E. Frida, P. Simamora, T. Sinaga, Analisis difraksi nanopartikel Fe3O4 metode kopresipitasi dengan polietilen glikol 6000, Seminar Nasional Fisika 4 (2015) 163–166.

[11] J. Huang, W. Liu, Y. Liang, L. Li, L. Duan, J. Chen, F. Zhu, Y. Lai, W. Zhu, W. You, Z.F. Jia, J. Xiong, D. Wang, Preparation and biocompatibility of diphasic magnetic nanocomposite scaffold, Mater. Sci. Eng. C 87 (2018) 70–77.

[12] L. Shen, B. Li, Y. Qiao, Fe3O4 nanoparticles in targeted drug/gene delivery systems, Materials 11 (2018) 324–352.

[13] X.F. Zhao, W.Y. Wang, X.D. Li, S.P. Li, F.G. Song, Core-shell structure of Fe3O4@MTX-LDH/Au NPs for cancer therapy, Mater. Sci. Eng. C 89 (2018) 422–428.

[14] G. Wang, D. Zhao, N. Li, X. Wang, Y. Ma, Drug-loaded poly (ε-caprolactone)/Fe3O4 composite microspheres for magnetic resonance imaging and controlled drug delivery, J. Magn. Magn Mater. 456 (2018) 316–323.

[15] Y. Yew, K. Shameli, M. Miyake, K.N. Ahmad, S. Mohamad, T. Naiki, K. Lee, Green biosynthesis of superparamagnetic magnetite Fe_3O_4 nanoparticles and biomedical applications in targeted anticancer drug delivery system: a review *Arabian*, J. Chem. 13 (2018) 2287–2308.

[16] R. Massart, Preparation of aqueous magnetic liquids in alkaline and acidic media, IEEE Trans. Magn. 17 (1981) 1247–1248.

[17] J. Kim, V.T. Tran, S. Oh, C.-S. Kim, J.C. Hong, S. Kim, Y.-S. Joo, S. Mun, M.-H. Kim, J.-W. Jung, Scalable solvothermal synthesis of superparamagnetic Fe3O4 nanoclusters for bioseparation and theragnostic probes, ACS Appl. Mater. Interfaces 10 (2018) 41935–41946.

[18] P. Lorkit, M. Panapoy, B. Ksapabutr, Iron oxide-based supercapacitor from ferratrane precursor via sol–gel-hydrothermal Process, Energy Procedia 56 (2014) 466–473.

[19] S.H. Chaki, T.J. Malek, M.D. Chaudhary, J.P. Tailor, M.P. Deshpande, Magnetite Fe_3O_4 nanoparticles synthesis by wet chemical reduction and their characterization, Adv. Nat. Sci. Nanosci. Nanotechnol. 6 (2015) 1–6, 035009.

[20] M. Aliahmad, M.N. Nasiri, Synthesis of maghemite (γ-Fe_2O_3) nanoparticles by thermal-decomposition of magnetite (Fe_3O_4) nanoparticles, Mater. Sci.-Poland 31 (2013) 264–268.

[21] Y. Zhao, J. Li, L. Zhao, S. Zhang, Y. Huang, X. Wu, X. Wang, Synthesis of amidoxime-functionalized Fe_3O_4@SiO_2 core–shell magnetic microspheres for highly efficient sorption of U(VI), Chem. Eng. J. 235 (2014) 275–283.

[22] S. Zhang, Q. Fan, H. Gao, Y. Huang, X. Liu, J. Li, X. Xu, X. Wang, Formation of Fe_3O_4@MnO_2 ball-in-ball hollow spheres as a high performance catalyst with enhanced catalytic performances, J. Mater. Chem. 4 (2016) 1414–1422.

[23] W. Jiang, J. Wu, Y. Shen, R. Tian, S. Zhou, W. Jiang, Synthesis and characterization of doxorubicin loaded pH-sensitive magnetic core–shell nanocomposites for targeted drug delivery applications, Nano 11 (2016) 1–23, 1650127.

[24] M. Gao, W. Li, J. Dong, Z. Zhang, B. Yang, Synthesis and Characterization of superparamagnetic Fe_3O_4/SiO_2 core-shell composite nanoparticles *World*, J. Condens. Matter Phys. 1 (2011) 49–54.

[25] S. Vinayasree, T.S. Nitha, C.S. Tiwary, P.M. Ajayan, P.A. Joy, M.R. Anantharaman, Magnetically tunable liquid dielectric with giant dielectric permittivity based on core–shell superparamagnetic iron oxide, Nanotechnology 29 (2018) 1–21, 265707.

[26] T.T. Baby, S. Ramaprabhu, SiO_2 coated Fe_3O_4 magnetic nanoparticle dispersed multiwalled carbon nanotubes based amperometric glucose biosensor, Talanta 80 (2010) 2016–2022.

[27] I. Stambolova, S. Yordanov, L. Lakov, S. Vassilev, V. Blaskov, B. Jivov, Preparation of sol-gel SiO2 coatings on steel and their corrosion resistance, MATEC Web Confer. 145 (2018) 1–7, 05011.

[28] Z. Cai, Y. Wei, M. Wu, Y. Guo, Y. Xie, R. Tao, R. Li, P. Wang, A. Ma, H. Zhang, Lipase immobilized on layer-by-layer polysaccharide-coated Fe_3O_4@SiO_2 microspheres as a reusable biocatalyst for the production of structured lipids, ACS Sustain. Chem. Eng. 7 (2019) 6685–6695.

[29] R. Thenmozhi, M.S. Moorthy, J. Sivaguru, P. Manivasagan, S. Bharathiraja, Y.-O. Oh, J. Oh, Synthesis of silica-coated magnetic hydroxyapatite composites for drug delivery applications, J. Nanosci. Nanotechnol. 19 (2019) 1951–1958.

[30] H. Shao, J. Qi, T. Lin, Y. Zhou, Preparation and characterization of Fe_3O_4@SiO_2@NMDP core-shell structure composite magnetic nanoparticles, Ceram. Int. 44 (2018) 2255–2260.

[31] L.F. Lai, H.X. Guo, Preparation of new 5-fluorouracil-loaded zein nanoparticles for liver targeting, Int. J. Pharm. 404 (2011) 317–323.

[32] W. Cai, M. Guo, X. Weng, W. Zhang, Z. Chen, Adsorption of doxorubicin hydrochloride on glutaric anhydride functionalized Fe_3O_4@SiO_2 magnetic nanoparticles, Mater. Sci. Eng. C 98 (2019) 65–73.

[33] C.-W. Zhang, C.-C. Zeng, Y. Xu, Preparation and characterization of surface-functionalization of silica-coated magnetite nanoparticles for drug delivery, Nano 9 (2014) 1–8, 1450042.

[34] S. Ullah, K. Seidel, S. Türkkan, D.P. Warwas, T. Dubich, M. Rohde, H. Hauser, P. Behrens, A. Kirschning, M. Köster, D. Wirth, Macrophage entrapped silica coated superparamagnetic iron oxide particles for controlled drug release in a 3D cancer model, J. Contr. Release 294 (2019) 327–336.

[35] M. Niu, M. Du, Z. Gao, C. Yang, X. Lu, R. Qiao, M. Gao, Monodispersed magnetic polystyrene beads with excellent colloidal stability and strong magnetic response, Macromol. Rapid Commun. 31 (2010) 1805–1810.

[36] G. Li, B. Shen, N. He, C. Ma, S. Elingarami, Z. Li, Synthesis and characterization of Fe_3O_4@SiO_2 core–shell magnetic microspheres for extraction of genomic DNA from human whole blood, J. Nanosci. Nanotechnol. 11 (2011) 10295–10301.

[37] J. Zhang, S. Zhai, S. Li, Z. Xiao, Y. Song, Q. An, G. Tian, Pb(II) removal of Fe_3O_4@SiO_2–NH_2 core–shell nanomaterials prepared via a controllable sol–gel process, Chem. Eng. J. 215–216 (2013) 461–471.

[38] A. Taufiq, S. Bahtiar, S. Sunaryono, N. Hidayat, A. Fuad, M. Diantoro, A. Hidayat, S. Pratapa, D. Darminto, Analysis of crystal structure and dielectric of Zn^{2+} ion doped nanoparticle magnetite based on iron sand synthesized by coprecipitation method *Indonesian*, J. Mater. Sci. 13 (2012) 153–156.

[39] Munasir, A. Terraningtyas, Synthesis and characterization of Fe_3O_4/SiO_2 composite with in-situ method: TEOS as SiO_2 NPs precursor *IOP Conference Series*, J. Phys. 1171 (2019) 1–5, 012050.

[40] Y. Chi, Q. Yuan, Y. Li, J. Tu, L. Zhao, N. Li, X. Li, Synthesis of Fe_3O_4@SiO_2–Ag magnetic nanocomposite based on small-sized and highly dispersed silver nanoparticles for catalytic reduction of 4-nitrophenol, J. Colloid Interface Sci. 383 (2012) 96–102.

[41] Munasir, A.S. Dewanto, D.H. Kusumawati, N.P. Putri, A. Yulianingsih, I.K.F. Sa'adah, A. Taufiq, N. Hidayat, S. Sunaryono, Z.A.I. Supardi, Structure analysis of Fe_3O_4@SiO_2 core shells prepared from amorphous and crystalline SiO_2 particles, IOP Conf. Ser. Mater. Sci. Eng. 367 (2018) 1–8, 012010.

[42] Munasir, A.S. Dewanto, A. Yulianingsih, I.K.F. Sa'adah, Z.A.I. Supardi, A. Mufid, A. Taufiq, Composites of Fe3O4/SiO2 from natural material synthesized by co-precipitation method, IOP Conf. Ser. Mater. Sci. Eng. 202 (2017) 1–6, 012057.

[43] E. Karimi Pasandideh, B. Kakavandi, S. Nasseri, A.H. Mahvi, R. Nabizadeh, A. Esrafili, R. Rezaei Kalantary, Silica-coated magnetite nanoparticles core-shell spheres (Fe_3O_4@SiO_2) for natural organic matter removal, J. Environ. Health Sci. Eng. 14 (2016) 1–13.

[44] M. Stjerndahl, M. Andersson, H.E. Hall, D.M. Pajerowski, M.W. Meisel, R.S. Duran, Superparamagnetic Fe_3O_4/SiO_2 nanocomposites: enabling the tuning of both the iron oxide load and the size of the nanoparticles, Langmuir 24 (2008) 3532–3536.

[45] Y. Junejo, A. Baykal, H. Sözeri, Simple hydrothermal synthesis of Fe_3O_4-PEG nanocomposite, Open Chem. 11 (2013) 1527–1532.

[46] D.V. Quy, N.M. Hieu, P.T. Tra, N.H. Nam, N.H. Hai, N. Thai Son, P.T. Nghia, N.T.V. Anh, T.T. Hong, N.H. Luong, Synthesis of silica-coated magnetic nanoparticles and application in the detection of pathogenic viruses, J. Nanomater. 2013 (2013) 1–6, 603940.

[47] C. Kurniawan, A.S. Eko, Y.S. Ayu, P.T.A. Sihite, M. Ginting, P. Simamora, P. Sebayang, Synthesis and characterization of magnetic elastomer based PEG-coated Fe_3O_4 from natural iron sand, IOP Conf. Ser. Mater. Sci. Eng. 202 (2017) 1–7, 012051.

[48] F. Ahangaran, A. Hassanzadeh, S. Nouri, Surface modification of Fe_3O_4@SiO_2 microsphere by silane coupling agent, Int. Nano Lett. 3 (2013) 23–27.

[49] K. Zomorodian, H. Veisi, S.M. Mousavi, M.S. Ataabadi, S. Yazdanpanah, J. Bagheri, A.P. Mehr, S. Hemmati, H. Veisi, Modified magnetic nanoparticles by PEG-400-immobilized Ag nanoparticles (Fe_3O_4@ PEG–Ag) as a core/shell nanocomposite and evaluation of its antimicrobial activity, Int. J. Nanomed. 13 (2018) 3965–3973.

[50] A.R. Rouhani, A.H. Esmaeil-Khanian, F. Davar, S. Hasani, The effect of agarose content on the morphology, phase evolution, and magnetic properties of CoFe2O4 nanoparticles prepared by sol-gel autocombustion method International, J. Appl. Ceramic Technol. 15 (2018) 758–765.

[51] M.S. Beg, J. Mohapatra, L. Pradhan, D. Patkar, D. Bahadur, Porous Fe3O4-SiO2 core-shell nanorods as high-performance MRI contrast agent and drug delivery vehicle, J. Magn. Magn Mater. 428 (2017) 340–347.

[52] S. Yang, T. Zeng, Y. Li, J. Liu, Q. Chen, J. Zhou, Y. Ye, B. Tang, Preparation of graphene oxide decorated Fe_3O_4@SiO_2 nanocomposites with superior adsorption capacity and SERS detection for organic dyes, J. Nanomater. 16 (2015) 817924 1–8.

[53] Y. Rangraz, F. Nemati, A. Elhampour, Organoselenium–palladium(ii) complex immobilized on functionalized magnetic nanoparticles as a promising retrievable nanocatalyst for the "phosphine-free" Heck–Mizoroki coupling reaction, New J. Chem. 42 (2018) 15361–15371.

[54] M. Emadi, E. Shams, M.K. Amini, Removal of zinc from aqueous solutions by magnetite silica core-shell nanoparticles, J. Chem. 2013 (2013) 1–10.

[55] E. Alzahrani, Photodegradation of binary azo dyes using core-shell Fe_3O_4/SiO_2/TiO_2 nanospheres, Am. J. Anal. Chem. 8 (2017) 95–115.

[56] L.D. Setiawati, Ekstraksi titanium dioksida (TiO2) Dari pasir besi dengan metode hidrometalurgi Prosiding, SEMIRATA 1 (2013) 465–467.

[57] S. Duan, X. Xu, X. Liu, Y. Wang, T. Hayat, A. Alsaedi, Y. Meng, J. Li, Highly enhanced adsorption performance of U(VI) by non-thermal plasma modified magnetic Fe_3O_4 nanoparticles, J. Colloid Interface Sci. 513 (2018) 92–103.

[58] A. Raghunath, E. Perumal, Metal oxide nanoparticles as antimicrobial agents: a promise for the future, Int. J. Antimicrob. Agents 49 (2017) 137–152.
[59] D.E. Camporotondi, M.L. Foglia, G.S. Alvarez, A.M. Mebert, L.E. Diaz, T. Coradin, M.F. Desimone, Antimicrobial properties of silica modified nanoparticles *microbial* Pathogens and Strategies for combating them: science, Technology and education, Microbiol. Book Ser. (2013) 283–290.
[60] N.E.A. El-Gamel, L. Wortmann, K. Arroub, S. Mathur, SiO_2@Fe_2O_3 core–shell nanoparticles for covalent immobilization and release of sparfloxacin drug, Chem. Commun. 47 (2011) 10076–10078.
[61] Y. Liu, L. He, A. Mustapha, H. Li, Z.Q. Hu, M. Lin, Antibacterial activities of zinc oxide nanoparticles against Escherichia coli O157: H7, J. Appl. Microbiol. 107 (2009) 1193–1201.
[62] M.D. Popova, Á. Szegedi, I.N. Kolev, J. Mihály, B.S. Tzankov, G.T.Z. Momekov, N.G. Lambov, K.P. Yoncheva, Carboxylic modified spherical mesoporous silicas as drug delivery carriers, Int. J. Pharm. 436 (2012) 778–785.
[63] E. Li, Y. Yang, G. Hao, X. Yi, S. Zhang, Y. Pan, B. Xing, M. Gao, Multifunctional magnetic mesoporous silica nanoagents for *in vivo* enzyme-responsive drug delivery and MR imaging, Nanotheranostics 2 (2018) 233–242.
[64] N. Gan, P. Xiong, J. Wang, T. Li, F. Hu, Y. Cao, L. Zheng, A novel signal-amplified immunoassay for the detection of C-reactive protein using HRP-doped magnetic nanoparticles as Labels with the Electrochemical Quartz Crystal Microbalance as a Detector, J. Analyt. Method Chem. 2013 (2013) 1–8, 482316.
[65] X. Weng, W. Cai, S. Lin, Z. Chen, Degradation mechanism of amoxicillin using clay supported nanoscale zero-valent iron, Appl. Clay Sci. 147 (2017) 137–142.
[66] S. Mortazavi-Derazkola, M. Salavati-Niasari, H. Khojasteh, O. Amiri, S.M. Ghoreishi, Green synthesis of magnetic Fe_3O_4/SiO_2/HAp nanocomposite for atenolol delivery and in vivo toxicity study, J. Clean. Prod. 168 (2017) 39–50.
[67] D. Deepika, J. PonnanEttiyappan, Synthesis and characterization of microporous hollow core-shell silica nanoparticles (HCSNs) of tunable thickness for controlled release of doxorubicin, J. Nanoparticle Res. 20 (2018), 187 1-15.